Available online at www.sciencedirect.com
SCIENCE DIRECT®
Journal of Power Sources 137 (2004) 183–195
JOURNAL OF POWER SOURCES
www.elsevier.com/locate/jpowsour

Performance equations for cathodes in polymer electrolyte fuel cells with non-uniform water flooding in gas diffusers

Hsiao-Kuo Hsuen*

Department of Chemical Engineering, Yuan Ze University, Chung-Li, Taiwan 320, ROC

Received 2 April 2004; accepted 3 June 2004
Available online31 July 2004

Abstract

The performance equations for cathodes of polymer electrolyte fuel cells (PEFCs) that describe the dependence of cathode potential on current density are developed. Formulation of the performance equations starts from the reduction of a one-dimensional model that considers, in detail, the potential losses pertinent to the limitations of electron conduction, oxygen diffusion, proton migration, and the oxygen reduction reaction. In particular, non-uniform accumulation of liquid water in the gas diffuser, which partially blocks the gas channels and imposes a greater resistance for oxygen transport, is taken into account. Reduction of the one-dimensional model is implemented by approximating the oxygen concentration profile in the catalyst layer with a parabolic polynomial or a piecewise parabolic one determined by the occurrence of oxygen depletion. The final forms of the equations are obtained by applying the method of weighted residuals over the catalyst layer. The weighting function is selected in such a way that the weighted residuals can be analytically integrated. Potential losses caused by the various limiting processes can be quantitatively estimated by the performance equations. Thus, they provide a convenient diagnostic tool for the cathode performance. Computational results reveal that the performance equations agree well with the original one-dimensional model over an extensive range of parameter values. This indicates that the present performance equations can be used as a substitute for the one-dimensional model to provide quantitatively correct predictions for the cathode performance of PEFCs.

Keywords: Polymer electrolyte; Fuel cell; Performance equation; Polarization; Modeling

1. Introduction

The polymer electrolyte fuel cell (PEFC) is an electrical power generation device that operates with an ionomeric membrane as its electrolyte layer. The overall behaviour of PEFCs can be described by so-called 'performance curves', which reveal the dependence of cell voltage on operating current density. Such a characteristic curve is a conclusion of the interplay among all the transport and electrochemical processes that take place inside the PEFC. Since the dominant mechanism for the performance of a PEFC may shift from one to another, distinguished types of behaviour are observed for different regimes of operating current densities. At low current densities, a sharp decay in cell voltage is noted, which is caused by the limitations of the electrochemical reactions. These losses are also referred to as activation overpotential, which arises from the electrochemical reaction being driven from the equilibrium so as to generate electric currents. As the current density increases, the increasing rate of activation overpotential is alleviated and an almost linear regime appears for intermediate current densities. Such behaviour basically reveals the characteristics of ohmic losses due to proton migration in the membrane and in the ionomer phase of the catalyst layers as well as electron conduction through the catalysts and the gas diffusers. As the current density approaches its limiting value, potential losses due to mass-transport limitations take over. Under this condition, the chemical reaction is limited by the rate at which the reactants can be supplied and a fast decay of cell potential is observed in the performance curve.

In order to elucidate the behaviour of such a complex system, many research efforts in PEFC modelling have been made and are based on electrochemical kinetics, phenomenological transport, and the mass and energy conservation laws. As reported in the literature, the complexity of the PEFC models is extremely variable. Detailed considerations on geometrical configuration in PEFCs lead to three-dimensional models [1–4]. Two-dimensional models

* Tel.: +886-3-4638800x569; fax: +886-3-4559373.
E-mail address: skhsun@ce.yzu.edu.tw (H.-K. Hsuen).

0378-7753/$ – see front matter © 2004 Elsevier B.V. All rights reserved.
doi:10.1016/j.jpowsour.2004.06.002

Nomenclature

a	effective platinum surface area per unit volume ($cm^2\ cm^{-3}$)
A	parameter in capillary pressure head expression
b	dimensionless coordinate at the diffuser face
C	parameter in capillary pressure head expression
c_{O_2}	oxygen concentration ($mol\ cm^{-3}$)
$c_{O_2,ref}$	reference oxygen concentration ($mol\ cm^{-3}$), defined as P/H_{O_2}
d	gas-diffuser thickness (μm)
D	parameter in capillary pressure head expression (cm)
D^{eff}_{i-j}	effective binary diffusion coefficient for i and j species ($cm^2\ s^{-1}$)
D_{i-j}	binary diffusion coefficient for i and j species ($cm^2\ s^{-1}$)
$D^{eff}_{O_2}$	effective diffusivity of dissolved oxygen in the catalyst layer ($cm^2\ s^{-1}$)
F	Faraday's constant (96487 C per equivalent)
H_{O_2}	Henry's constant for oxygen ($atm\ cm^3\ mol^{-1}$)
$i_{o,ref}$	exchange current density at the reference condition ($A\ cm^{-2}$)
I	cathode current density ($A\ cm^{-2}$)
I_o	characteristic current density, defined by Eq. (16f) ($A\ cm^{-2}$)
k^{eff}_m	effective protonic conductivity for the ionomer phase ($S\ cm^{-1}$)
k^{eff}_d	effective electric conductivity for the gas diffuser ($S\ cm^{-2}$)
$K_{l,abs}$	liquid water permeability at 100% saturation (cm^2)
l_m	membrane thickness (μm)
N_i	mole flux of species i (mol per cm^2 s)
$N_{w,m}$	mole flux of water through the membrane|catalyst-layer interface (mol per cm^2 s)
n_d	electro-osmotic drag coefficient
m_w	molecular weight of water
p	parameter defined by Eq. (44)
P	total pressure (atm)
q_w	liquid water flux ($cm\ s^{-1}$)
r	parameter, defined by Eq. (32)
R	the universal gas constant (8.314 J per mol K)
s	liquid water saturation of diffuser, defined as $1-\varepsilon/\varepsilon_0$
T	cathode temperature (K)
V	catalyst potential (V)
V_c	cathode potential (V)
V_o	open-circuit potential (V)
w	dimensionless position where oxygen depletion occurs
x_i	mole fraction of species i
x^b_i	x_i in the bulk flow
x^c_i	x_i at the catalyst-layer|gas-diffuser interface
$x^m_{O_2}$	x_{O_2} at the catalyst-layer|membrane interface
z	coordinate perpendicular to the face of the gas diffuser (μm)

Greek letters

α_i	electrode transfer coefficient
β_1	parameter, defined by Eq. (16b) ($S\ cm^{-2}$)
β_2	parameter, defined by Eq. (23) ($S\ cm^{-2}$)
δ	the catalyst-layer thickness (μm)
ε	porosity of gas diffuser
ε_0	porosity of gas diffuser at zero water saturation
$\varepsilon_{w,m}$	volume fraction of water in membrane
ϕ	ionomer potential (V)
ϕ^c	ϕ at the gas-diffuser|catalyst-layer interface (V)
ϕ	parameter, defined by Eq. (16a)
Λ	parameter, defined by Eq. (41)
η	parameter, defined by Eq. (39)
λ	water content of membrane (moles of water per mole of sulfonic groups)
μ_w	viscosity of liquid water (g per cm s)
ρ_w	density of liquid water ($g\ cm^{-3}$)
τ_w	water mole flux driven by hydraulic permeation, defined by Eq. (6) (mol per cm^2 s)
ζ	dimensionless coordinate, defined by Eq. (2)

are formulated by considering the variations of state variables along the gas channel and along the direction normal to the gas diffuser [5–10]. There are also two-dimensional models with emphasis on the effects of local inhibition of oxygen transport on the face of the gas diffuser by ribbed carbon plates [11–13], or on the effects of interdigitated flow fields [14]. Because the cell thickness in PEFCs is orders of magnitude smaller than other dimensions, one-dimensional models, though simplified ones, are still able to provide a good account of the polarization behaviour of PEFCs. With different foci in investigations, a wide variety of one-dimensional models have also been proposed [15–23]. In addition, empirical or semi-empirical models characterized by algebraic equations have been suggested [24–30].

In general, a mechanistic model, which takes into account spatial variations of reactant concentration and potential, provides better insight into the involved physical and electrochemical phenomena, and hence better interpretation of experimental data. Such models can also be employed as a predictive tool since all model parameters have a precise physical meaning. The dependencies of the various sources

of polarization on the model parameters are described, however, by a set of coupled differential equations, and thus their effects on the cell performance cannot be clearly revealed. In addition, considerable efforts on modelling and computations, contingent upon the model complexity, are usually required.

The overall loss of voltage in PEFCs can be viewed as a summation of individual contributive terms that originate from limitations of reactant transport, proton migration, electron conduction, and the electrochemical reactions. This observation forms the basis for the formulation of most empirical and semi-empirical models [24–30]. In these formulations, the overall loss of cell voltage is expressed as a summation of a few terms that account for the characteristics of the losses of the potentials of the various limiting processes. Parameters without physical origin and significance are incorporated, and have to be determined by fitting the equations with experimental data. Consequently, empirical and semi-empirical models are only data-fitting tools and cannot be used for performance prediction, but they do provide simple algebraic expressions for the relation between the cell voltage and current density.

In previous work [31], the performance equations for PEFC cathodes were derived based on a mechanistic approach. The performance equations were formulated from the reduction of a one-dimensional model through approximating the profiles of oxygen concentration, catalyst potential and ionomer potential with appropriate parabolic functions and lumping the electrochemical reaction at a reaction centre. The analysis was further employed to formulate the performance equations of a single cell that included potential losses pertinent to its cathode, anode and membrane electrolyte [32]. The derived performance equations were characterized in an algebraic form as empirical models but with no appreciable degradation of accuracy. Nevertheless, in the previous studies, the details of liquid water transport in the gas diffuser were not considered. The transport of oxygen in the gas diffuser was characterized by a single value of the effective porosity of the diffuser, which was assumed to be invariant with current density. In practical situations, liquid water may accumulate in the gas diffuser. In addition, the profile of water saturation in the gas diffuser is not uniform, which also evolves with operating current density. The accumulated water partially obstructs the gas channels of the diffuser, and hence, imposes greater limitations for oxygen transport. The objective of the present study is to develop performance equations for PEFC cathodes that also take such phenomena into consideration. In addition, the method of weighted residuals [33,34] is applied over the catalyst-layer domain so as to yield the final forms of the performance equations. Compared with the performance equations developed previously, the ones presented here not only provide a deeper insight into the processes involved at a PEFC cathode but also allow for more accurate estimations of its overall performance.

2. One-dimensional model

The cathode considered in the present work consists of two parts, namely, a catalyst layer and a gas diffuser. These are illustrated in Fig. 1. The assumptions employed to derive the model equations are delineated as following:

(i) an isothermal, steady-state model is considered;
(ii) pressure variations within the gas diffuser are negligible;
(iii) the Stefan–Maxwell equations are employed for multi-component gas transport in the gas diffuser, and the Bruggeman expression [17], which includes the effects of porosity and tortuosity, is applied to evaluate the effective binary gas diffusivity;
(iv) as liquid water appears in the gas diffuser, the water vapour is assumed to be saturated;
(v) the nitrogen mole flux is zero due to its inertness;
(vi) catalyst particles and conductive ionomers are homogeneously mixed in the catalyst layer; a macro-homogeneous assumption is applied, which indicates that the local physical and chemical properties are invariant with position inside the catalyst layer;
(vii) the oxygen reduction reaction follows a first-order reaction rate expression with respect to oxygen concentration, and the reaction rate is described by the Butler–Volmer expression [35,36];
(viii) Henry's law holds for the phase equilibrium of oxygen at the gas-diffuser|catalyst-layer interface;
(ix) Fick's law is applied for the transport of oxygen within the catalyst layer and the oxygen flux is zero at the catalyst-layer|membrane interface;
(x) the loss in potential due to electron conduction in the catalyst layer is negligible.

These assumptions are basic ones implied in the model equations; others, which are not mentioned above, will be stated as they are employed in formulation.

With the assumptions stated above, the Stefan–Maxwell equations can be condensed to one single equation as liquid water prevails in the gas diffuser, i.e., [17]:

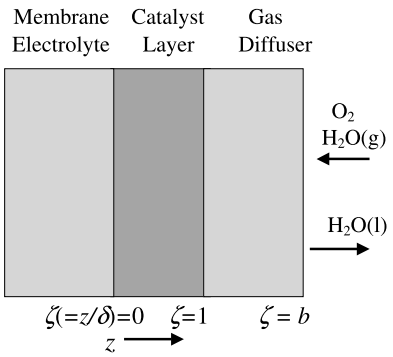

Fig. 1. Schematic of components and geometry considered for PEFC cathode.

$$\frac{P}{RT}\frac{\mathrm{d}x_{\mathrm{O_2}}}{\delta \mathrm{d}\zeta} = -(1 - x_{\mathrm{w}}^{\mathrm{b}} - x_{\mathrm{O_2}})N_{\mathrm{O_2}}\left[\frac{1}{D_{\mathrm{N_2-O_2}}^{\mathrm{eff}}} + \frac{x_{\mathrm{w}}^{\mathrm{b}}}{x_{\mathrm{O_2}}D_{\mathrm{w-N_2}}^{\mathrm{eff}} + (1 - x_{\mathrm{w}}^{\mathrm{b}} - x_{\mathrm{O_2}})D_{\mathrm{O_2-w}}^{\mathrm{eff}}}\right] \quad (1)$$

where N_i is the mole flux of species i; x_i is its mole fraction; D_{i-j}^{eff} is the effective gas-pair diffusivity for i and j species in the porous medium; R is the universal gas constant; P is the total pressure; T is the cathode temperature; δ is the thickness of the catalyst layer; ζ is the dimensionless coordinate defined as:

$$\zeta = \frac{z}{\delta} \quad (2)$$

where z is the coordinate perpendicular to the face of the gas-diffuser.

The steady-state assumption requires:

$$\frac{\mathrm{d}N_{\mathrm{O_2}}}{\mathrm{d}\zeta} = 0 \quad (3)$$

Generally, three different transport mechanisms are responsible for liquid water transport through the membrane|catalyst-layer interface; namely, electro-osmotic drag, hydraulic permeation by the pressure difference between two sides of the membrane, and back diffusion by the gradients of water concentration within the membrane. In the present work, the membrane is considered to be well hydrated and consequently the contribution attributed to back diffusion is neglected. Accordingly, the mole flux of liquid water transported through the membrane|catalyst-layer interface, denoted as $N_{\mathrm{w,m}}$, is expressed as [17,22]:

$$N_{\mathrm{w,m}} = n_{\mathrm{d}}\frac{I}{F} - \frac{\varepsilon_{\mathrm{w,m}}\rho_{\mathrm{w}}k_{\mathrm{p,m}}}{m_{\mathrm{w}}\mu_{\mathrm{w}}}\frac{\Delta P_{\mathrm{m}}}{l_{\mathrm{m}}} \quad (4)$$

where

$$n_{\mathrm{d}} = 2.5\frac{\lambda}{22} \quad (5)$$

For brevity, we assign

$$\tau_{\mathrm{w}} = \frac{\varepsilon_{\mathrm{w,m}}\rho_{\mathrm{w}}k_{\mathrm{p,m}}}{m_{\mathrm{w}}\mu_{\mathrm{w}}}\frac{\Delta P_{\mathrm{m}}}{l_{\mathrm{m}}} \quad (6)$$

In the above expressions, n_{d} is the electro-osmotic drag coefficient; λ is the water content in membrane; $k_{\mathrm{p,m}}$ is the membrane permeability; l_{m} is the membrane thickness; I is the current density; F is Faraday's constant; μ_{w} is the water viscosity; ρ_{w} is the water density; m_{w} is the molecular weight of water; $\varepsilon_{\mathrm{w,m}}$ is the volume fraction of water in the membrane; ΔP_{m} is the pressure difference between the two sides of membrane. Based on the above definitions, the value of $N_{\mathrm{w,m}}$ may be positive or negative contingent upon the combined contributions of these two mechanisms. A positive value implies that a net water flow is transported from the membrane to the catalyst layer, while a negative flow indicates that liquid water passes in the opposite direction.

Darcy's law is applied to describe the liquid water transport in the gas diffuser. Because it is postulated that the variations of gas pressure within the gas diffuser are negligible, the gradients of capillary pressure of the liquid phase become the only driving forces for water flow. Thus, the liquid water flux, q_{w}, is expressed as:

$$q_{\mathrm{w}} = -[(2 + 4n_{\mathrm{d}})N_{\mathrm{O_2}} + N_{\mathrm{w}} + \tau_{\mathrm{w}}]\left(\frac{m_{\mathrm{w}}}{\rho_{\mathrm{w}}}\right) = \frac{-K(s)\rho_{\mathrm{w}}g}{\mu_{\mathrm{w}}}\left(-\frac{\mathrm{d}\psi}{\mathrm{d}s}\right)\left(\frac{\mathrm{d}s}{\delta \mathrm{d}\zeta}\right) \quad (7)$$

where $K(s)$ is the diffuser permeability; ψ is the capillary head of liquid water; g is the gravitational acceleration; s is the water saturation of the diffuser. Taking the local saturation into account, the effective gas-pair diffusivity is evaluated as:

$$D_{i-j}^{\mathrm{eff}} = \varepsilon_0^{1.5}(1 - s)^{1.5}D_{i-j} \quad (8)$$

With the stated assumptions, the Stefan–Maxwell equations can be rearranged to give

$$N_{\mathrm{w}} = N_{\mathrm{O_2}}\left[\frac{D_{\mathrm{N_2-w}}^{\mathrm{eff}}x_{\mathrm{w}}^{\mathrm{b}}}{D_{\mathrm{N_2-w}}^{\mathrm{eff}}x_{\mathrm{O_2}} + D_{\mathrm{O_2-w}}^{\mathrm{eff}}(1 - x_{\mathrm{w}}^{\mathrm{b}} - x_{\mathrm{O_2}})}\right] = N_{\mathrm{O_2}}\left[\frac{D_{\mathrm{N_2-w}}x_{\mathrm{w}}^{\mathrm{b}}}{D_{\mathrm{N_2-w}}x_{\mathrm{O_2}} + D_{\mathrm{O_2-w}}(1 - x_{\mathrm{w}}^{\mathrm{b}} - x_{\mathrm{O_2}})}\right] \quad (9)$$

$K(s)$ and $\mathrm{d}\psi/\mathrm{d}s$ are expressed as [11]:

$$\frac{\mathrm{d}\psi}{\mathrm{d}s} = -AD[e^{-A(s-C)} + e^{A(s-C)}] \quad (10)$$

$$K(s) = K_{\mathrm{l,abs}}(s + 0.01) \quad (11)$$

Inserting Eqs. (9)–(11) into Eq. (7) results in

$$\left[2 + 4n_{\mathrm{d}} + \frac{D_{\mathrm{N_2-w}}x_{\mathrm{w}}^{\mathrm{b}}}{D_{\mathrm{N_2-w}}x_{\mathrm{O_2}} + D_{\mathrm{O_2-w}}(1 - x_{\mathrm{w}}^{\mathrm{b}} - x_{\mathrm{O_2}})}\right]N_{\mathrm{O_2}} + \tau_{\mathrm{w}} + \frac{K_{\mathrm{l,abs}}\rho_{\mathrm{w}}^2 gAD(s + 0.01)[e^{-A(s-C)} + e^{A(s-C)}]}{\mu_{\mathrm{w}}m_{\mathrm{w}}\delta} \times \left(\frac{\mathrm{d}s}{\mathrm{d}\zeta}\right) = 0 \quad (12)$$

In the catalyst layer ($0 < \zeta < 1$), the equations of mass conservation, electro-neutrality and Ohm's law can be expressed in a partially dimensionless form as:

$$\frac{\mathrm{d}^2x_{\mathrm{O_2}}}{\mathrm{d}\zeta^2} - \varphi\{\exp[f_{\mathrm{c}}(V_0 - V + \phi)] - \exp[-f_{\mathrm{a}}(V_0 - V + \phi)]\}x_{\mathrm{O_2}} = 0 \quad (13)$$

$$\frac{\mathrm{d}^2x_{\mathrm{O_2}}}{\mathrm{d}\zeta^2} - \frac{\beta_1}{I_o}\frac{\mathrm{d}^2\phi}{\mathrm{d}\zeta^2} = 0 \quad (14)$$

$$\frac{\mathrm{d}V}{\mathrm{d}\zeta} = 0 \quad (15)$$

The model parameters appearing in the above expressions are defined by:

$$\varphi = \frac{a i_{o,ref} H_{O_2} \delta^2}{4FPD^{eff}_{O_2}} \tag{16a}$$

$$\beta_1 = \frac{k^{eff}_m}{\delta} \tag{16b}$$

$$f_c = \frac{\alpha_c F}{RT} \tag{16c}$$

$$f_a = \frac{\alpha_a F}{RT} \tag{16d}$$

$$x_{O_2} = \frac{c_{O_2}}{c_{O_2,ref}} = \frac{c_{O_2}}{P/H_{O_2}} \tag{16e}$$

$$I_o = \frac{4FPD^{eff}_{O_2}}{H_{O_2}\delta} \tag{16f}$$

where α_i is the electrode transfer coefficient; a is the effective platinum surface area per unit volume; $i_{o,ref}$ is the exchange current density at the reference condition; c_{O_2} is the dissolved oxygen concentration in the ionomer phase; k^{eff}_m is the effective protonic conductivity for the ionomer phase; $D^{eff}_{O_2}$ is the effective diffusivity of dissolved oxygen in the catalyst layer; V_o is the open-circuit potential; V is the catalyst potential; ϕ is the ionomer potential; and H_{O_2} is Henry's constant for gaseous oxygen and its dissolved form in the ionomer phase at the cathode temperature. It should be noted that x_{O_2} stands for the oxygen mole fraction in the gas phase of the diffuser, but represents the dimensionless concentration of dissolved oxygen in the ionomer phase within the catalyst layer as defined by Eq. (16e). The same symbol was used in both of the two regions because, by such definitions, the x_{O_2} profiles are continuous across their boundary.

At the face of the gas diffuser ($\zeta = b$), Eq. (3) is also applied. Other boundary conditions are:

$$x_{O_2} = x^b_{O_2} \tag{17}$$

$$s = 0 \tag{18}$$

At the gas-diffuser|catalyst-layer interface ($\zeta = 1$), in addition to Eq. (3), other conditions are written as

$$x_{O_2}(\text{catalyst layer}) = x_{O_2}(\text{gas diffuser}) \tag{19}$$

$$\frac{I_o}{4F}\frac{dx_{O_2}}{d\zeta}(\text{catalyst layer}) = -N_{O_2} \tag{20}$$

$$\frac{d\phi}{d\zeta} = 0 \tag{21}$$

The cathode potential (denoted as V_c) is equivalent to the catalyst potential deducted by the ohmic loss of the diffuser. Thus, one has:

$$V_c = V(\text{catalyst}) - \left(-\frac{4FN_{O_2}}{\beta_2}\right) \tag{22}$$

and

$$\beta_2 = \frac{k^{eff}_d}{d} \tag{23}$$

where k^{eff}_d is the effective electric conductivity of the gas diffuser and d is its thickness.

At the membrane|catalyst-layer interface ($\zeta = 0$), in addition to Eq. (15), the boundary conditions are formulated as:

$$\phi = 0 \tag{24}$$

$$\frac{dx_{O_2}}{d\zeta} = 0 \tag{25}$$

The one-dimensional model derived above forms a three-point boundary value problem with three governing equations and three state variables in each domain. Eqs. (1), (3) and (12) are applied for the diffuser where state variables x_{O_2}, N_{O_2} and s are present. Eqs. (13)–(15) are employed for the catalyst layer, and in the region state variables x_{O_2}, ϕ and V appear. The method of collocation on finite elements based on cubic B-spline interpolation was used to solve the model equations [37]. Forty sub-intervals with equal size were arranged in the domain of the gas diffuser. The domain of the catalyst layer was also divided into the same number of sub-intervals; but the size of the sub-intervals was decreased along the ζ direction with a common ratio of 0.7 to account for the extremely high oxygen concentration gradients that develop in a narrow region near the gas-diffuser|catalyst-layer interface at high current densities. Two points were collocated in each sub-interval, which thus transform the model equations into a set of algebraic equations. Newton's method was employed for the solutions of the discretized equations.

At low current densities, where liquid water has not yet appeared within the diffuser, the Stefan–Maxwell equations take the forms:

$$\frac{P}{RT}\frac{dx_{N_2}}{\delta d\zeta} = x_{N_2}\left[\frac{N_{O_2}}{D^{eff}_{N_2-O_2}} + \frac{N_W}{D^{eff}_{w-N_2}}\right] \tag{26}$$

$$\frac{P}{RT}\frac{dx_{O_2}}{\delta d\zeta} = \frac{x_{O_2}}{D^{eff}_{O_2-w}}(N_{O_2} + N_w) + x_{N_2}N_{O_2} \times \left(\frac{1}{D^{eff}_{O_2-w}} - \frac{1}{D^{eff}_{N_2-O_2}}\right) - \frac{N_{O_2}}{D^{eff}_{O_2-w}} \tag{27}$$

Under such a condition, $q_w = 0$ and Eq. (7) becomes:

$$(2 + 4n_d)N_{O_2} + N_w + \tau_w = -(2 + 4n_d)\frac{I}{4F} + N_w + \tau_w = 0 \tag{28}$$

and N_w can be expressed as:

$$N_w = (2 + 4n_d)\frac{I}{4F} - \tau_w \tag{29}$$

Eq. (26) can be solved to give

$$x_{N_2} = x^{b}_{N_2} \exp\left[\frac{\delta RT}{P}\left(\frac{N_{O_2}}{D^{eff}_{N_2-O_2}} + \frac{N_W}{D^{eff}_{w-N_2}}\right)(\zeta - b)\right] \quad (30)$$

After inserting Eq. (30), Eq. (27) can be solved to give:

$$\begin{aligned} x_{O_2} = {} & \left[x^{b}_{O_2} - \frac{x^{b}_{N_2} N_{O_2}}{-N_{O_2} + rN_w} - \frac{N_{O_2}}{N_{O_2} + N_w}\right] \\ & \times \exp\left[\frac{\delta RT}{PD^{eff}_{O_2-w}}(N_{O_2} + N_w)(\zeta - b)\right] \\ & + \frac{x^{b}_{N_2} N_{O_2}}{-N_{O_2} + rN_w} \exp\left[\frac{\delta RT}{P}\left(\frac{N_{O_2}}{D^{eff}_{N_2-O_2}} + \frac{N_W}{D^{eff}_{w-N_2}}\right)\right. \\ & \left. \times (\zeta - b)\right] + \frac{N_{O_2}}{N_{O_2} + N_w} \end{aligned} \quad (31)$$

where:

$$r = \frac{D^{eff}_{O_2-N_2}(D^{eff}_{O_2-w} - D^{eff}_{N_2-w})}{D^{eff}_{N_2-w}(D^{eff}_{N_2-O_2} - D^{eff}_{O_2-w})} \quad (32)$$

With the employment of Eq. (29) and assigning ζ to 1, the value of x_{O_2} at the gas-diffuser|catalyst-layer interface, denoted as $x^{c}_{O_2}$, can be obtained as:

$$\begin{aligned} x^{c}_{O_2} = {} & \frac{-x^{b}_{N_2} I}{I + r[(4n_d + 2)I - 4F\tau_w]} \\ & \times \exp\left\{-\frac{dRT}{4FP}\left[\frac{-I}{D^{eff}_{N_2-O_2}} + \frac{(4n_d + 2)\, I - 4\tau_w F}{D^{eff}_{w-N_2}}\right]\right\} \\ & + \left\{x^{b}_{O_2} + \frac{x^{b}_{N_2} I}{I + r[(4n_d + 2)I - 4F\tau_w]}\right. \\ & \left. + \frac{I}{(4n_d + 1)I - 4\tau_w F}\right\} \\ & \times \exp\left\{-\frac{dRT[(4n_d + 1)I - 4\tau_w F]}{4FPD^{eff}_{O_2-w}}\right\} \\ & - \frac{I}{(4n_d + 1)I - 4\tau_w F} \end{aligned} \quad (33)$$

By similar procedures, the value of x_{N_2} at the gas-diffuser|catalyst-layer interface, represented as $x^{c}_{N_2}$, is calculated as:

$$x^{c}_{N_2} = x^{b}_{N_2} \exp\left\{-\frac{dRT}{4FP}\left[\frac{-I}{D^{eff}_{N_2-O_2}} + \frac{(4n_d + 2)I - 4\tau_w F}{D^{eff}_{w-N_2}}\right]\right\} \quad (34)$$

Under such a condition, the model equations for the gas diffuser can be solved analytically. Consequently, the numerical approach described above is applied for the catalyst-layer domain only. Starting from $I = 0$, x^{c}_{w} $(= 1 - x^{c}_{O_2} - x^{c}_{N_2})$ is lower than x^{b}_{w} due to hydraulic permeation of liquid water through the membrane. Under this condition, $x^{c}_{O_2}$ is evaluated by using Eq. (33). As I is increased, x^{c}_{w} increases also. When it reaches x^{b}_{w}, liquid water starts to appear in the diffuser. Then, the three-point boundary value problem formulated above has to be solved to construct the remainder of the polarization curve of the PEFC cathode.

3. Formulation of performance equations

With the approximation $D^{eff}_{N_2-w} \cong D^{eff}_{O_2-w}$, Eq. (12) can be simplified to:

$$\begin{aligned} & \left[2 + 4n_d + \frac{x^{b}_{w}}{1 - x^{b}_{w}}\right] N_{O_2} + \tau_w \\ & + \frac{K_{l,abs}\rho^2_w gAD(s + 0.01)[e^{-A(s-C)} + e^{A(s-C)}]}{\mu_w m_w \delta} \\ & \times \left(\frac{ds}{d\zeta}\right) = 0 \end{aligned} \quad (35)$$

Then, integrating over the diffuser domain leads to:

$$\begin{aligned} & \frac{\{I[2 + 4n_d + x^{b}_{w}/(1 - x^{b}_{w})] - 4\tau_w F\} m_w \mu_w d}{4FK_{l,abs}\rho^2_w gAD} \\ & = -\exp[-AC]\left(\frac{0.01}{A} - \frac{1}{A^2}\right) + \exp[AC]\left(\frac{0.01}{A} + \frac{1}{A^2}\right) \\ & \quad + \exp[A(s^c - C)]\left(\frac{s^c + 0.01}{A} - \frac{1}{A^2}\right) \\ & \quad - \exp[-A(s^c - C)]\left(\frac{s^c + 0.01}{A} + \frac{1}{A^2}\right) \end{aligned} \quad (36)$$

where s^c represents the value of s at the gas-diffuser|catalyst-layer interface. Using the same approximation, Eq. (1) is simplified to:

$$\begin{aligned} \frac{P}{RT}\frac{dx_{O_2}}{\delta d\zeta} = {} & -(1 - x^{b}_{w} - x_{O_2})N_{O_2} \\ & \times \left[\frac{1}{D^{eff}_{N_2-O_2}} + \frac{x^{b}_{w}}{(1 - x^{b}_{w})D^{eff}_{O_2-w}}\right] \end{aligned} \quad (37)$$

Inserting Eq. (35) into Eq. (37) results in

$$\frac{dx_{O_2}}{(1 - x^{b}_{w} - x_{O_2})} = -\eta\frac{(s + 0.01)\left[e^{-A(s-C)} + e^{A(s-C)}\right]ds}{(1 - s)^{1.5}} \quad (38)$$

where:

$$\begin{aligned} \eta = {} & \frac{K_{l,abs}RTADg\rho^2_w}{Pm_w\mu_w\varepsilon_0^{1.5}[2 + 4n_d + x^{b}_{w}/(1 - x^{b}_{w}) - 4\tau_w F/I]} \\ & \times \left[\frac{1}{D_{N_2-O_2}} + \frac{x^{b}_{w}}{(1 - x^{b}_{w})D_{O_2-w}}\right] \end{aligned} \quad (39)$$

Integration of Eq. (38) over the diffuser yields:

$$x^{c}_{O_2} = x^{b}_{O_2} - x^{b}_{N_2}[\exp(\eta\Lambda) - 1] \tag{40}$$

in which

$$\Lambda = -\int_{s^c}^{0} \frac{(s+0.01)[e^{-A(s-C)} + e^{A(s-C)}]}{(1-s)^{1.5}} ds \tag{41}$$

With a given value of s^c, Λ can be evaluated using the formula of Gauss quadrature [34]. The number of interior points required to yield an accurate estimation of Λ strongly depends on the value of s^c. Only two points are required for a value of s^c close to zero. For a larger value of s^c, more points must be considered. As it will be shown in the base case in the following section, s^c is increased to 0.95 while the limiting current is approached. Under this condition, the employment of 10 interior points is able to yield an estimate with desired accuracy. Accordingly, the formula of Gauss quadrature with 10 interior points is used to evaluate Λ in all calculations of the present work. If liquid water has not yet appeared in the diffuser (low current densities), using the approximation $D^{eff}_{N_2-w} \cong D^{eff}_{O_2-w}$ ($r = 0$), Eq. (33) can be simplified to:

$$x^{c}_{O_2} = -x^{b}_{N_2} \exp\left\{\frac{-dRT}{4FP}\left[\frac{-I}{D^{eff}_{N_2-O_2}} + \frac{(4n_d+2)I - 4\tau_w F}{D^{eff}_{w-N_2}}\right]\right\} - \frac{I}{(4n_d+1)I - 4\tau_w F} + \left\{x^{b}_{O_2} + x^{b}_{N_2} + \frac{I}{(4n_d+1)I - 4\tau_w F}\right\} \times \exp\left\{\frac{-dRT[(4n_d+1)I - 4\tau_w F]}{4FPD^{eff}_{O_2-w}}\right\} \tag{42}$$

It is further assumed that the dimensionless oxygen concentration profile in the catalyst layer be approximated by a parabolic function, which has the form:

$$x_{O_2} = p\zeta^2 + x^{c}_{O_2} - p \tag{43}$$

Eq. (43) automatically satisfies the boundary conditions required by the profile of x_{O_2} at $\zeta = 0$ and 1. Because the current density is equivalent to the flux of dissolved oxygen at the catalyst-layer|gas-diffuser interface multiplied by $-4F$, p can be expressed as:

$$p = \frac{I}{2I_o} \tag{44}$$

Integration of Eq. (14) along the ζ direction twice leads to:

$$\phi = \frac{I_o}{\beta_1}\left(x_{O_2} - x^{m}_{O_2} - \frac{I}{I_o}\zeta\right) \tag{45}$$

where $x^{m}_{O_2}$ stands for the oxygen concentration at the membrane|catalyst-layer interface and is evaluated as:

$$x^{m}_{O_2} = x^{c}_{O_2} - \frac{I}{2I_o} \tag{46}$$

Neglecting the anodic rate in Eq. (13), inserting Eq. (45), multiplying $(dx_{O_2}/d\zeta)\exp(f_c I\zeta/\beta_1)$ and then integrating over the catalyst-layer domain, one eventually arrives at:

$$\int_0^1 \frac{d^2x_{O_2}}{d\zeta^2}\frac{dx_{O_2}}{d\zeta}\exp\left(\frac{f_c I}{\beta_1}\zeta\right)d\zeta - \varphi\exp\left[f_c\left(V_o - V - \frac{I_o}{\beta_1}x^{c}_{O_2} + \frac{I}{2\beta_1}\right)\right] \times \int_{x^{m}_{O_2}}^{x^{c}_{O_2}} \exp\left(\frac{f_c I_o}{\beta_1}x_{O_2}\right)x_{O_2}dx_{O_2} = 0 \tag{47}$$

With the incorporation of Eqs. (43)–(46), Eq. (47) can be analytically integrated. After certain algebraic rearrangements, the cathode potential is expressed as

$$V_c = V_o - \frac{I}{2\beta_1} - \frac{I}{\beta_2} - \frac{1}{f_c}\ln\left\{\frac{I + \beta_1/f_c\left[\exp(-If_c/\beta_1) - 1\right]}{\varphi[I_o x^{c}_{O_2} - (\beta_1/f_c) + \exp(-If_c/2\beta_1) \times ((\beta_1/f_c) - I_o x^{c}_{O_2} + (I/2))]}\right\} \tag{48}$$

The above derivation procedures basically follow the principles of the method of weighted residuls [33,34]. The weighting function $(dx_{O_2}/d\zeta)\exp((f_c I/\beta_1)\zeta)$ is used in order to fulfil analytical integration of the weighted residual.

The overall potential loss in a PEFC cathode is a summation of the individual contributive terms, which include diffusion overpotential and ohmic overpotential for electron conduction in the diffusion layer, diffusion overpotential and ohmic potential loss for proton migration in the catalyst layer, and activation overpotential for the electrochemical reaction. Remember, the ohmic potential loss caused by electron conduction in the catalyst layer is not taken into account in the present study due to its negligible value. The activation overpotential is referred to as the potential loss required to generate the desired current density under the condition without any transport limitations and ohmic losses. Thus, it is quantified as:

$$\text{activation overpotential for electrochemical reaction} = \frac{1}{f_c}\ln\left(\frac{I}{\varphi x^{b}_{O_2} I_o}\right) \tag{49}$$

The diffusion overpotential of the gas diffuser arises from the difference in oxygen concentration at the diffuser face and at the catalyst-layer|gas-diffuser interface, which is expressed as:

$$\text{diffusion overpotential in gas diffuser} = \frac{1}{f_c}\ln\left(\frac{x^{b}_{O_2}}{x^{c}_{O_2}}\right) \tag{50}$$

The ohmic loss caused by proton migration in the catalyst layer is calculated as the difference of ionomer po-

tential at the membrane|catalyst-layer interface and at the catalyst-layer|gas-diffuser interface, which has the form:

$$\text{ohmic loss (protonic) in catalyst layer} = \frac{I}{2\beta_1} \tag{51}$$

The potential loss due to electron conduction in the gas diffuser is determined by Ohm's law as:

$$\text{ohmic loss (electronic) in gas diffuser} = \frac{I}{\beta_2} \tag{52}$$

The remaining part of Eq. (48) is attributed to the diffusion overpotential in the catalyst layer, which is calculated as:

$$\text{diffusion overpotential in catalyst layer} = \frac{1}{f_c}\ln\left\{\frac{1+\beta_1/If_c[\exp(-If_c/\beta_1)-1]}{[1-(\beta_1/f_cI_ox^c_{O_2})+\exp(-If_c/2\beta_1)\times((\beta_1/f_cI_ox^c_{O_2})-1+(I/2I_ox^c_{O_2}))]}\right\} \tag{53}$$

Eq. (43) is physically meaningful only for the condition that $x^m_{O_2}$ is greater than zero, which indicates:

$$I \le 2I_ox^c_{O_2} \tag{54}$$

As the current density exceeds the critical value, Eq. (43) is no longer applicable and Eq. (48) is not valid either. Under such a condition, we propose to employ a piecewise parabolic function for the dimensionless oxygen concentration profile within the catalyst layer, which is:

$$x_{O_2} = x^c_{O_2}\left(\frac{\zeta-w}{1-w}\right)^2, \quad \text{for } w \le \zeta \le 1 \quad \text{and}$$
$$x_{O_2} = 0, \quad \text{for } 0 \le \zeta \le w \tag{55}$$

where w is the dimensionless position in the catalyst layer where oxygen depletion takes place. Relating the transport rate of dissolved oxygen at the catalyst-layer|gas-diffuser interface to the electric current density of the cathode gives:

$$w = 1 - \frac{2x^c_{O_2}I_o}{I} \tag{56}$$

Based on the proposed profile function for x_{O_2} within the catalyst layer, Eq. (48) has to be reformulated as:

$$\int_w^1 \frac{d^2x_{O_2}}{d\zeta^2}\frac{dx_{O_2}}{d\zeta}\exp\left(\frac{If_c}{\beta_1}\zeta\right)d\zeta - \varphi\exp[f_c(V_o-V)] \times \int_0^{x^c_{O_2}}\exp\left(\frac{I_of_c}{\beta_1}x_{O_2}\right)x_{O_2}dx_{O_2} = 0 \tag{57}$$

After inserting Eqs. (55) and (56), Eq. (57) can be analytically integrated. With certain algebraic operations, the cathode potential has the form:

$$V_c = V_o - \frac{I}{\beta_1} + \frac{x^c_{O_2}I_o}{\beta_1} - \frac{I}{\beta_2} - \frac{1}{f_c}\ln\left\{\frac{I^2[2x^c_{O_2}I_of_c-\beta_1+\beta_1\exp(-2x^c_{O_2}I_of_c/\beta_1)]}{4\varphi(x^c_{O_2})^2I_o^2[x^c_{O_2}I_of_c-\beta_1+\beta_1\exp(-x^c_{O_2}I_of_c/\beta_1)]}\right\} \tag{58}$$

The diffusion overpotential and the ohmic loss of the gas diffuser, as well as the activation overpotential for the oxygen reduction reaction, all have the same forms as the previous case. Other contributive terms for potential loss are modified as

$$\text{diffusion overpotential of catalyst layer} = \frac{1}{f_c}\ln\left\{\frac{I[2x^c_{O_2}I_of_c-\beta_1+\beta_1\exp(-2x^c_{O_2}I_of_c/\beta_1)]}{4x^c_{O_2}I_o[x^c_{O_2}I_of_c-\beta_1+\beta_1\exp(-x^c_{O_2}I_of_c/\beta_1)]}\right\} \tag{59}$$

$$\text{ohmic loss (protonic) in the catalyst layer} = \frac{I}{\beta_1} - \frac{x^c_{O_2}I_o}{\beta_1} \tag{60}$$

4. Validation of performance equations

In order to investigate the validity of the parabolic approximation employed in formulation, polarization curves based on the one-dimensional model and the performance equations derived previously have been calculated over an extensive range of the values of the model parameters. Since an analytical form of the exact solutions of the one-dimensional model is not available, we consider its numerical solutions as exact ones in comparisons. In order to carry out the comparisons over a wide parameter range, the parameter values listed in Table 1 are taken as a base case. Calculations were implemented by adjusting the value of a particular parameter in the table while keeping other ones unchanged. It is noted that the effective oxygen diffusivity in the catalyst layer ($D^{eff}_{O_2}$) listed in Table 1 is larger than the value for fully hydrated Nafion® 117 [17]. Such a selection was based on the consideration of the presence of small amounts of gas pores in the catalyst layer that might greatly enhance oxygen transport. The parameter values related to the capillary pressure of the gas diffuser were taken from the work of Natarajan and Nguyen [11], in which the cathode operating temperature is 60 °C. Due to the weak temperature dependence of these parameters [11], they were directly used for the base case without any modifications.

The polarization curves calculated using the performance equations and the one-dimensional model for the base case are illustrated in Fig. 2. As it shows, these two curves

Table 1
Values of model parameters for the base case

Effective ionic conductivity of ionomer, k_m^{eff} (S cm^{-1})	3×10^{-2}
Effective electric conductivity of gas diffuser, k_d^{eff} (S cm^{-1})	1
Effective diffusivity of dissolved oxygen in the catalyst layer, $D_{O_2}^{eff}$ (cm^2 s^{-1})	1×10^{-5}
Gas-pair diffusivity, $D_{O_2-N_2}$ (cm^2 s^{-1})	5.58×10^{-2}
Gas-pair diffusivity, D_{N_2-w} (cm^2 s^{-1})	7.74×10^{-2}
Gas-pair diffusivity, D_{O_2-w} (cm^2 s^{-1})	7.40×10^{-2}
Gas-diffuser thickness, d (μm)	200
Catalyst-layer thickness, δ (μm)	10
Porosity of gas diffuser at zero water saturation, ε_0	0.6
Product of platinum surface area and reference exchange current, $ai_{o,ref}$ (A cm^3)	1×10^{-2}
Pressure, P (atm)	5
Bulk oxygen mole fraction, $x_{O_2}^b$	0.190
Bulk nitrogen mole fraction, $x_{N_2}^b$	0.716
Bulk mole fraction of water vapor, x_w^b (relative humidity, 100%)	0.094
Temperature, T (°C)	80
Henry's constant, H_{O_2} (atm cm^3 per mol)	2.0×10^5 [17]
Open-circuit potential, V_o (V)	1.197 [17]
Cathodic transfer coefficient, α_c	1.0
Anodic transfer coefficient, α_a	0.5
Membrane thickness, l_m (μm)	230 [17]
Pressure difference between two sides of membrane, ΔP_m (atm)	2
Hydraulic permeability of membrane, $k_{p,m}$ (cm^2)	1.58×10^{-14} [17]
Water viscosity, μ_w (g cm^{-1} s^{-1})	3.565×10^{-3}
Volume fraction of water in membrane, $\varepsilon_{w,m}$	0.28 [17]
Density of liquid water, ρ_w (g cm^{-3})	0.972
Liquid water permeability of diffuser 100% saturation, $K_{l,abs}$ (cm^2)	3×10^{-10}
Constants in capillary head expression A, C and D in cm	3.7, 0.494 and 0.0173 [11]
Water content in membrane under saturated water vapor (moles of water per mole of sulfonic groups), λ	14 [22]

are well matched. For the parameter values employed in calculations, liquid water starts to appear in the gas diffuser at $I = 0.26\,A\,cm^{-2}$. The profiles of liquid saturation in the gas diffuser for four selected current densities are illustrated in Fig. 3. As shown, when the current density approaches its limiting value, the water saturation at the gas-diffuser|catalyst-layer interface reaches the value of 0.95. Such an observation is consistent with the low value of the limiting current observed in Fig. 2. For the sake of simplicity, a single value of ionic conductivity for the ionomer phase of the catalyst layer was employed in calculations for the entire range of current density. In fact, the value of k_m^{eff} depends on the degree of hydration of the ionomer phase. The computational results reveal that the mole fraction of water vapour at the catalyst-layer|gas-diffuser interface is 19% lower than the saturated value at $I = 0$ due to hydraulic

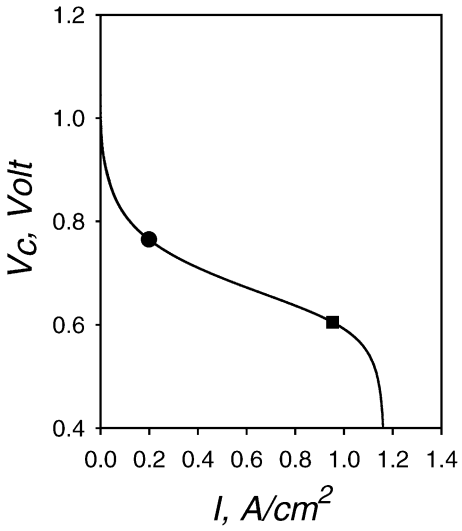

Fig. 2. Polarization curves for base case: (●) one-dimensional model and (■) performance equations.

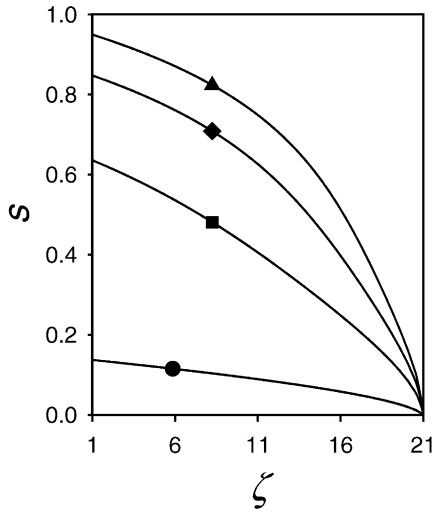

Fig. 3. Profiles of water saturation within diffuser at various current densities: (●) $I = 0.30\,A\,cm^{-2}$; (■) $I = 0.58\,A\,cm^{-2}$; (◆) $I = 0.89\,A\,cm^{-2}$; and (▲) $I = 1.17\,A\,cm^{-2}$.

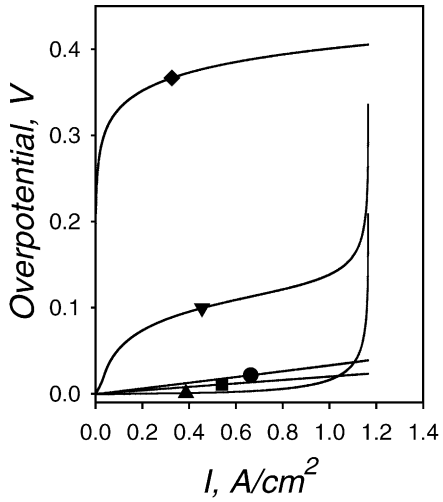

Fig. 4. Polarization curves of individual contributive terms for base case calculated using performance equations: (◆) activation overpotential for oxygen reduction reaction; (▼) diffusion overpotential of catalyst layer; (▲) diffusion overpotential of gas diffuser; (●) ohmic potential loss of ionomer phase in catalyst layer; and (■) ohmic potential loss of gas diffuser.

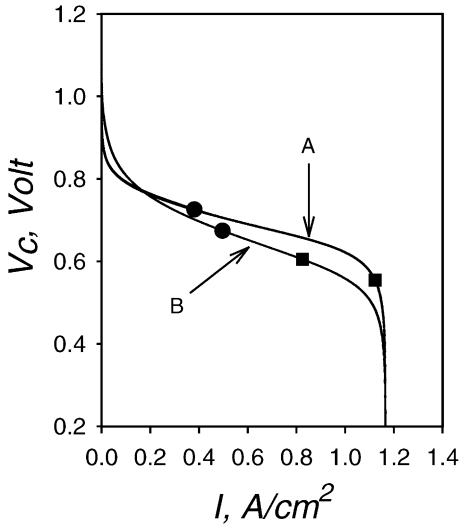

Fig. 5. Polarization curves for cathodes with different catalyst-layer thicknesses: (A) $\delta = 1\,\mu m$; (B) $\delta = 20\,\mu m$; (●) one-dimensional model; and (■) performance equations.

permeation of liquid water through the membrane. This fact also leads to a lower degree of hydration and, hence, a lower ionic conductivity of the ionomer phase in the catalyst layer. As the current density becomes higher, x_w^c is increased and the value of k_m^{eff} also becomes larger. Because such phenomena only exist in the region of low current densities, the errors caused by ignoring the variations of k_m^{eff} in calculations would not be significant as long as the difference between x_w^b and x_w^c at $I = 0$ is not large.

The individual potential losses caused by the limitations of oxygen reduction kinetics, oxygen transport, proton migration, and electron conduction for the base case are presented in Fig. 4. These were calculated based on the derived performance equations. As illustrated, the activation overpotential for the oxygen reduction reaction increases sharply as the current density is driven away from zero. Its increasing rate is alleviated as the current density is further increased. Such a behaviour can be clearly revealed by the logarithmic dependence of the activation overpotential on current density, as shown by Eq. (49). The potential losses caused by proton migration in the ionomer phase of the catalyst layer and by electron conduction in the gas diffuser form the major part of the overall ohmic loss of the cathode. The potential loss of the gas diffuser is linear with current density, as revealed by Ohm's law. Up to the occurrence of oxygen depletion in the catalyst layer, the potential loss of ionomer phase is also linear with current density as shown by Eq. (51). After this point, its expression becomes a function of $x_{O_2}^c$ [Eq. (60)]. The diffusion overpotential evolves with the current density in a more complicated fashion. It increases with the current density and goes sharply to infinity as the limiting current is approached. Such a phenomenon is also noted for the diffusion overpotential of the gas diffuser and stems from the depletion of oxygen concentration at the catalyst-layer|gas-diffuser interface.

The thickness of the catalyst layer may vary by some orders of magnitude, as dictated by the preparation methods and by the amounts of catalysts and ionomers used. A thickness of less than 1 μm is achievable by sputtering [38]. When a catalyst layer is prepared by printing or brushing an ionomer|carbon-supported-platinum ink on to a membrane, the thickness of the layer formed is much larger. The results displayed in Fig. 5 were calculated for two cathodes with two different values of catalyst-layer thickness, namely, 1 and 20 μm. These two values were selected with an intention to cover the wide variations in catalyst-layer thickness that result from the different nature of fabrication techniques. As shown, the polarization curves obtained using the performance equations agree well with those from the one-dimensional model. At low current densities, where oxygen is able to reach the membrane|catalyst–layer interface, a thicker catalyst layer implies that larger space is available to accommodate the oxygen reduction reaction. Consequently, a lower activation overpotential is needed to generate the required electric current. In other respects, a higher ohmic loss for proton migration is formed for a thicker catalyst layer due to a longer travel distance. Besides, a higher diffusion overpotential is expected due to a lower value of the average oxygen concentration over the catalyst layer. At low densities, where the oxygen depletion has not yet occurred, the effect of the first factor overshadows the other two, and thus results in better performance for the cathode with a thicker catalyst layer. Nevertheless, after the onset of oxygen depletion, the influence of the first factor diminishes and the other two take over. Accordingly, the cathode with a thinner catalyst layer exhibits a higher cathode potential at intermediate and high current densities.

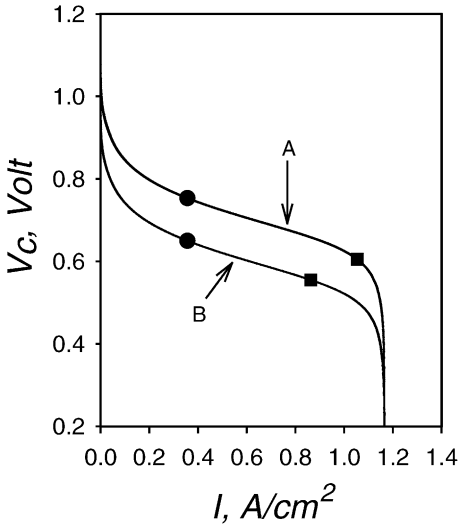

Fig. 6. Polarization curves for the cathodes with different product values of $ai_{o,ref}$: (A) $ai_{o,ref} = 3 \times 10^{-2}\,A\,cm^{-3}$; (B) $ai_{o,ref} = 1 \times 10^{-3}\,A\,cm^{-3}$; (●) one-dimensional model; and (■) performance equations.

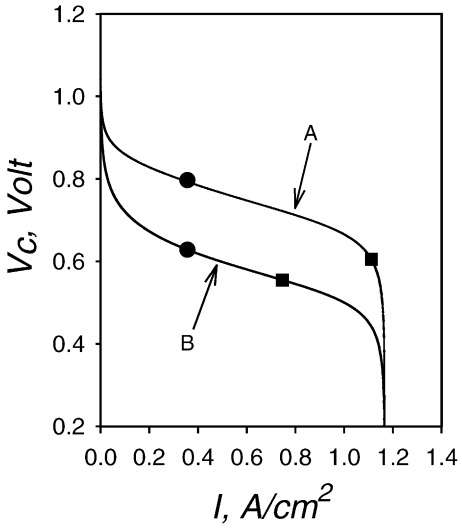

Fig. 7. Polarization curves for cathodes with different values of effective oxygen diffusivity in catalyst layer: (A) $D^{eff}_{O_2} = 1 \times 10^{-4}\,cm^2\,s^{-1}$; (B) $D^{eff}_{O_2} = 5 \times 10^{-7}\,cm^2\,s^{-1}$; (●) one-dimensional model; and (■) performance equations.

Investigation of the discrepancies between the polarization curves calculated based on the derived performance equations and on the one-dimensional model was carried out for two cathodes with different products values of $ai_{o,ref}$, i.e., 3×10^{-2} and $1 \times 10^{-3}\,A\,cm^{-3}$. The results are presented in Fig. 6. A rather good agreement is also found between these two models, as in the previous case. In the model equations, the product value of $ai_{o,ref}$ quantifies the overall reactivity of the catalyst layer, which includes the intrinsic activity of the catalysts and the active surface area available for the occurrence of the oxygen reduction reaction. For a cathode with a lower value of $ai_{o,ref}$, a higher activation overpotential is required to generate the identical electric current; thus, a lower cathode potential results. As shown in Fig. 6, the cathode with a higher product value of $ai_{o,ref}$ outperforms the one with a lower $ai_{o,ref}$ value for the entire range of current density.

For all model parameters appearing in the performance equations, $D^{eff}_{O_2}$ is practically the one that exerts the major influence on the diffusion overpotential of the catalyst layer. The value of $D^{eff}_{O_2}$ is greatly influenced by the presence of a small amount of gas pores in the layer. In order to take this factor into consideration, two $D^{eff}_{O_2}$ values that differed by a factor of 200, namely, $D^{eff}_{O_2} = 1 \times 10^{-4}$ and $5 \times 10^{-7}\,cm^2\,s^{-1}$ were employed for calculations. The results are presented in Fig. 7. As seen, a fairly good agreement is found between the results from the performance equations and from the one-dimensional model. A higher $D^{eff}_{O_2}$ suggests that oxygen is able to diffuse into the inner part of the catalyst layer and, consequently, a lower diffusion overpotential results. This, in turn, yields a better performance for the cathode. Since the limiting current is determined by the oxygen transport in the diffuser, it is not influenced by the value of the effective diffusivity in the catalyst layer. As shown, the polarization curves for these two cases exhibit the same limiting value of current density.

Polarization curves are shown in Fig. 8 for two cathodes that were constructed with different values of the effective ionomer conductivity in the catalyst layer. As illustrated, the results are almost identical. Moreover, the cathode with $k^{eff}_m = 0.05\,S\,cm^{-1}$ always exhibits a better performance than the one with $k^{eff}_m = 0.01\,S\,cm^{-1}$ for the same current density. It should be noted that both the ohmic loss by proton migration and the oxygen diffusion overpotential are influenced by the value of k^{eff}_m, as revealed by Eqs. (51),

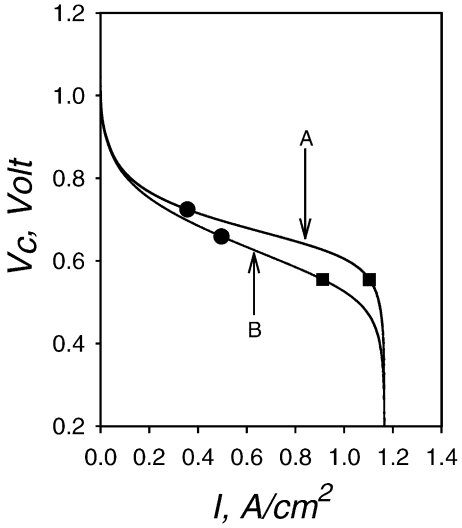

Fig. 8. Polarization curves for cathodes with different values of effective proton conductivity of ionomer phase in catalyst layer: (A) $k^{eff}_m = 0.05\,S\,cm^{-1}$; (B) $k^{eff}_m = 0.01\,S\,cm^{-1}$; (●) one-dimensional model; and (■) performance equations.

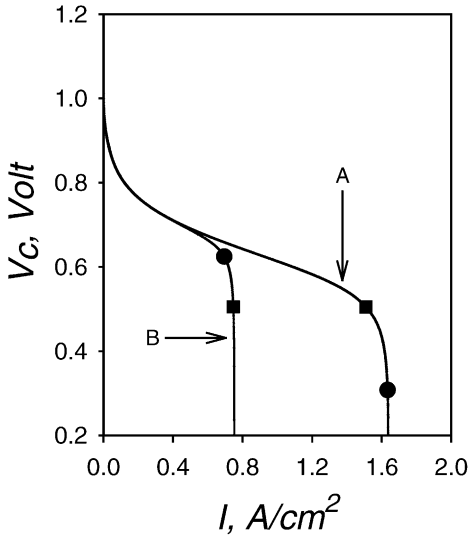

Fig. 9. Polarization curves for cathodes with different values of $K_{l,abs}$: (A) $K_{l,abs} = 5 \times 10^{-10}\,cm^2$; (B) $K_{l,abs} = 1.5 \times 10^{-10}\,cm^2$; (●) one-dimensional model; and (■) performance equations.

(53), (59) and (60). The former appears as the outcome of Ohm's law, while the latter arises from the participation of the ionomer potential in the oxygen reduction reaction.

As liquid water starts to appear in the gas-diffuser|catalyst-layer interface, it leaves the catalyst layer via the gas diffuser by a slow capillary process. The liquid water that accumulates in the gas diffuser partially obstructs the gas channels and hence imposes a greater resistance for oxygen transport. In addition to the gradients of capillary pressure head, the permeability of the diffuser plays an important role in liquid water transport. The polarization curves for the cathodes with two different $K_{l,abs}$ values were calculated based on the one-dimensional model and the performance equations. As shown in Fig. 9, the result obtained from the two models are nearly same. At low current densities, where there is no liquid water in the diffuser, the performances of the two cathodes are identical. After the onset of water accumulation in the diffuser, the cathode with $K_{l,abs} = 5 \times 10^{-10}\,cm^2$ yields a higher potential than that with $K_{l,abs} = 1.5 \times 10^{-10}\,cm^2$. This is because the former allows a greater transport rate of liquid water. It is also noted that the value of $K_{l,abs}$ significantly influences the magnitude of the limiting current density, and the limiting values can be accurately estimated using Eqs. (36) and (40).

In contrast to the performance equations developed previously [31], those present here provide a detailed physical insight into the liquid water transport within the gas diffuser. As to the approximation method employed in the catalyst-layer domain, it is also necessary to address the discrepancies between the present approach based on the method of weighted residuals and the previous ones that employed a lumping technique. This is because both yield highly accurate estimations of the cathode performance for the range of parameters under investigation. Compared with the ones derived previously using a piecewise linear approximation for the profile of the ionomer potential, the first notable feature is that these two approaches yield quite different forms for the diffusion overpotential of the catalyst layer. The previous approach gives rather simple expressions, which are independent of k_m^{eff}. By contrast, much more complex functions of effective ionomer conductivity are generated by the present analysis. In order to resolve such dissimilarity, we consider the following identity:

$$V_c = V_o + \phi^c - \frac{I}{\beta_2} + \frac{1}{f_c}\ln\left\{\frac{I}{x_{O_2}^c \varphi I_o \exp[f_c(V_o - V_c - I/\beta_2 + \phi^c)]}\right\} - \frac{1}{f_c}\ln\left(\frac{x_{O_2}^b}{x_{O_2}^c}\right) - \frac{1}{f_c}\ln\left(\frac{I}{x_{O_2}^b \varphi I_o}\right) \quad (61)$$

where ϕ^c denotes the ionomer potential at the gas-diffuser|catalyst-layer interface. With the aid of Eq. (61), the physical significance of the diffusion overpotential of the catalyst layer can be clearly revealed, that is equal to $-1/f_c$ multiplied by the logarithm of the effectiveness factor of the catalyst layer. The latter factor is defined as the ratio of actual current density to that evaluated based on the condition at the catalyst-layer|gas-diffuser interface. Due to the participation of ϕ^c in the expression for the catalyst-layer diffusion overpotential, it is expected that its value will also vary with k_m^{eff}. Such a dependency is eliminated, however, by the linear approximations that have been employed in the previous work. Another discrepancy in the expressions of ohmic loss of the ionomer phase in the catalyst layer stems from the different ionomer potential profiles employed in theses two approaches. In another model reported in the previous work, the parabolic profiles for ionomer potential only serve as a vehicle for evaluating the ionomer potential at the reaction centre, and the potential loss of the ionomer phase of the catalyst layer is calculated as the difference of ionomer potential at the reaction centre and at the catalyst-layer|membrane interface. In addition to a better revelation of parameter dependencies, the present performance equations also yield more accurate results than those developed earlier.

5. Summary and conclusions

In the present study, the performance equations for PEFC cathodes are formulated from the reduction of a one-dimensional model that takes into account the transport and electrochemical processes within the catalyst layer and the gas diffuser. In particular, the transport of liquid water in the gas diffuser and its effects on the polarization characteristics of the PEFC cathodes are considered. The reduction procedures are performed by employing a parabolic approximation or a piecewise parabolic one for

the oxygen concentration profile within the catalyst layer depending on the occurrence of oxygen depletion. Through the use of these approximations and an appropriate weighting function, analytic integration over the catalyst layer can be carried out, which leads to final expressions of the performance equations. Individual overpotential terms, which result from the limiting processes considered in the original one-dimensional model, can be quantitatively estimated by the equations. Computational results have shown that the polarization curves created by the performance equations and by the one-dimensional model agree well for the extensive parameter range investigated. With a clear revelation of parameter dependencies and a great reduction in computational efforts, the present performance equations provide an efficient tool for performance prediction and diagnosis of PEFC cathodes.

Acknowledgements

Financial support from Energy Commission, Ministry of Economic Affairs, Taiwan, ROC (contract no. 92-D0122) is gratefully acknowledged.

References

[1] T. Berning, D.M. Lu, N. Djilali, J. Power Sources 106 (2002) 284.
[2] S. Dutta, S. Shimpalee, J.W. Van Zee, J. Appl. Electrochem. 30 (2000) 135.
[3] T.-C. Jen, T. Yan, S.-H. Chan, Int. J. Heat Mass Transfer 46 (2003) 4157.
[4] D. Natarajan, T.V. Nguyen, J. Power Sources 115 (2003) 66.
[5] L. You, H. Liu, Int. J. Heat Mass Transfer 45 (2002) 2277.
[6] S. Um, C.-Y. Wang, K.S. Chen, J. Electrochem. Soc. 147 (2000) 4485.
[7] V. Gurau, H. Liu, S. Kakac, AIChE J. 44 (1998) 2410.
[8] T.F. Fuller, J. Newman, J. Electrochem. Soc. 140 (1993) 1218.
[9] J.S. Yi, T.V. Nguyen, J. Electrochem. Soc. 145 (1998) 1149.
[10] Z.H. Wang, C.Y. Wang, K.S. Chen, J. Power Sources 94 (2001) 40.
[11] D. Natarajan, T.V. Nguyen, J. Electrochem. Soc. 148 (2001) A1324.
[12] A.A. Kulikovsky, J. Divisek, A.A. Kornyshev, J. Electrochem. Soc. 146 (1999) 3981.
[13] A.C. West, T.F. Fuller, J. Appl. Electrochem. 26 (1996) 557.
[14] W. He, J.S. Yi, T.V. Nguyen, AIChE J. 46 (2000) 2053.
[15] M. Eikerling, A.A. Kronyshev, J. Electroanal. Chem. 453 (1998) 89.
[16] G. Murgia, L. Pisani, M. Valentini, B. D'Aguanno, J. Electrochem. Soc. 149 (2002) A31.
[17] D.M. Bernardi, M. Verbrugge, AIChE J. 37 (1991) 1151.
[18] D.M. Bernardi, M. Verbrugge, J. Electrochem. Soc. 139 (1992) 2477.
[19] C. Marr, X. Li, J. Power Sources 77 (1999) 17.
[20] A. Rowe, X. Li, J. Power Sources 102 (2001) 82.
[21] T.E. Springer, M.S. Wilson, S. Gottesfeld, J. Electrochem. Soc. 140 (1993) 3513.
[22] T.E. Springer, T.A. Zawodzinski, S. Gottesfeld, J. Electrochem. Soc. 138 (1991) 2334.
[23] F. Gloaguen, P. Convert, S. Gamburzev, O.A. Velve, S. Srinivasan, Electrochim. Acta 43 (1998) 3767.
[24] J. Kim, S.-M. Lee, S. Srinivasan, C.E. Chamberlin, J. Electrochem. Soc. 142 (1995) 2670.
[25] G. Squadrito, G. Maggio, E. Passalacqua, F. Lufrano, A. Patti, J. Appl. Electrochem. 29 (1999) 1449.
[26] J.H. Lee, T.R. Lalk, A.J. Appleby, J. Power Sources 70 (1998) 258.
[27] J.C. Amphlett, R.M. Baumert, R.F. Mann, B.A. Peppley, P.R. Roberge, T.J. Harris, J. Electrochem. Soc. 142 (1995) 1.
[28] J.C. Amphlett, R.M. Baumert, R.F. Mann, B.A. Peppley, P.R. Roberge, T.J. Harris, J. Electrochem. Soc. 142 (1995) 9.
[29] R.F. Mann, J.C. Amphlett, M. Hooper, H.M. Jensen, B.A. Peppley, P.R. Roberge, J. Power Sources 86 (2000) 173.
[30] L. Pisani, G. Murgia, M. Valentini, B. D'Aguanno, J. Power Sources 108 (2002) 192.
[31] H.-K. Hsuen, J. Power Sources 123 (2003) 26.
[32] H.-K. Hsuen, J. Power Sources 126 (2004) 46.
[33] B.A. Finlayson, The Method of Weighted Residuals and Variational Principles with Application in Fluid Mechanics, Heat and Mass Transfer, Academic Press, New York, 1972.
[34] J. Villadsen, M. L. Michelsen, Solution of Differential Equation Models by Polynomial Approximation, Prentice-Hall, Englewood Cliffs, NJ, 1978.
[35] A.J. Bard, L.R. Faulkner, Electrochemical Methods, Wiley, New York, 1980.
[36] J. Newman, Electrochemical Systems, Prentice-Hall, Englewood Cliffs, NJ, 1973.
[37] C. de Boor, A Practical Guide to Splines, Springer-Verlag, New York, 1978.
[38] S. Hirano, J. Kim, S. Srinivasan, Electrochim. Acta 42 (1997) 1587.